Hindawi
International Transactions on Electrical Energy Systems
Volume 2022, Article ID 3663237, 18 pages
https://doi.org/10.1155/2022/3663237

WILEY | Hindawi

Research Article

Fuzzy Fractional-Order PID Control for PMSG Based Wind Energy Conversion System with Sparse Matrix Converter Topology

Waleed Khaled Abdulrazaq Abdulrazaq and Ahmet Mete Vural

Electrical and Electronics Engineering Department, Engineering Faculty, Gaziantep University, Gaziantep 27310, Turkey

Correspondence should be addressed to Ahmet Mete Vural; mvural@gantep.edu.tr

Received 5 September 2022; Revised 17 October 2022; Accepted 26 October 2022; Published 7 November 2022

Academic Editor: Sujin Bureerat

Sparse matrix converter (SMC) is an indirect AC-to-AC power electronic converter that has a fictitious DC link between rectification and inversion stages in which neither a capacitor nor an inductor, as the storage element, is utilized. Due to this advantage, SMC is used in AC drives, marine thrust systems, aerospace industry, as well as in wind energy applications. On the other hand, permanent magnet synchronous generator (PMSG) is competitive in wind turbine applications due to their prominent features. In this work, a fuzzy fractional-order PID (FFOPID) controller is designed for a PMSG based wind energy conversion system (WECS) which employs a three-phase three-level SMC. The FFOPID controller is chosen to combine the salient features of the fractional-order calculus and fuzzy logic operations to enhance the dynamic response of classical PID controller with fixed gains. The simulation results taken under different case studies are analyzed in detail, which demonstrate the superiority of the designed FFOPID controller over classical PID control approach in tracking d- and q-axis current references of the SMC at the output. With the designed control approach, the smooth control of the real and reactive power injections into the grid from the WECS are ensured with acceptable transient response.

1. Introduction

Matrix converter (MC) is a power electronic AC-to-AC converter without any DC storage element such as capacitor or inductor. This adaptation reduces converter size, upsurges converter reliability, as well as provides four-quadrant operation [1–3]. Due to these salient features, MCs have been used in many applications such as AC drives, marine propulsion systems, aerospace industry, and renewable energy systems [4]. Recently, MCs have gained increased interest in wind energy applications [5]. In [6], different control strategies for MC topologies for wind energy applications are reviewed and an ultra-modified space vector modulation (SVM) scheme is proposed for a direct MC topology to reduce the harmonic content of output waveforms of a wind energy conversion system (WECS). A DFIG driven WECS, where a direct MC is connected to the rotor is suggested in [7]. In this study, the real as well as reactive power output of the WECS are controlled using sliding mode control approach. The simulation studies verify the usefulness of the sliding mode control method. In [8], the investigation of an offshore WECS with a high frequency link that consists of a permanent magnet synchronous generator (PMSG), a converter, a high frequency transformer, and a diode bridge rectifier is carried out. Various MC and back-to-back converter topologies are studied to compare the efficiency of each setup. On the other hand, sparse MC (SMC) is a member of MC family, in which indirect power conversion is realized using rectifier and inverter stages separated by a fictious DC link without any DC storage element [9]. The control complexity of the power semiconductor switches in SMC is a challenging task, since switching synchronization between rectifier and inverter stages is needed [4]. SMC has also found application areas in WECS. A three-level SMC is adopted to a grid-connected doubly fed induction generator (DFIG) based WECS in [10]. The simulation results affirm the suitability of the SMC to WECS applications in terms of control performance. A SMC topology as a variable speed

drive for a PMSG driven WECS is proposed in [11,12]. In both of these studies, SMC switches are modulated using SVM. An ultra-sparse MC topology is adopted for PMSG based WECS in [13].

In this study, a direct torque control mechanism is designed based on SVM to control rotor speed with reduced torque ripples. Numerous controllers are also suggested by researchers to retain the control variables of PMSG based WECS at the reference values against plant uncertainty and external disturbances. Studies employing conventional AC-to-AC converters having a real DC link with an energy storage element are plentiful. Recently, a sliding mode controller is designed for an offshore PMSG-WECS with conventional AC-to-AC conversion scheme to reduce the chattering issue [14]. The simulated cases illustrate that the proposed control method improves the robustness and stability of the system in the area of maximum power point tracking (MPPT). An adaptive control arrangement, which is based on the combination of PI control and adaptive filtering algorithm, is proposed in [15] to improve the MPPT and fault ride-through ability of grid-connected PMSG-WECS in which a conventional AC-to-AC conversion scheme is used. A Takagi-Sugeno fractional order (FO) fuzzy logic control strategy is proposed for a PMSG-WECS with a conventional AC-to-AC converter in [16]. Numerical simulations show the efficacy of the proposed control method. A conventional AC-to-AC converter is suggested in [17] for a PMSG fed WECS. In that study, a model predictive control strategy based on a finite control set is suggested for the converter regulation task. The numerical simulations demonstrate that the DC link voltage between the converters can heal under grid faults. A few control design studies has been proposed for WECS employing SMC topology. A PI controller is used to regulate the electromagnetic torque of PMSG driven WECS in which SMC is utilized [11]. In [18], a carrier based PWM technique is adopted for a SMC based PMSG-WECS, which is PI controlled. It is shown that the proposed control system is successful in real power control and oscillation damping for current/voltage waveforms of SMC. In the above literature scan, it is evident that in control design studies for PMSG-WECS, mostly the converter type is conventional in which a real dc link with an energy storage element exists between rectifier and inverter stages. On the other hand, PID controller is effective and can be easily implemented in many control areas. Moreover, there is a possibility to embed fractional calculus into control systems [19–21]. For example, FO based PID controller can give better results for nonlinear complex systems if carefully tuned when compared to classical PID control scheme [22–24]. Classical PID controller contains proportional gain, integral gain, and derivative gain. However, two additional parameters, such as integer term and differentiator term, exist in FOPID control structure. With the addition of these parameters, it has been shown that the response of the control system can be improved by using FOPID controllers [25–28]. Recent studies have shown that fuzzy logic can also be integrated to FO controllers to tune gains dynamically [16,29–31]. The present work is devoted to the utilization of a FOPID controller with a Mamdani type fuzzy logic scheme to improve the dynamic performance of the inverter stage controller for a SMC in PMSG-WECS. In the proposed control approach, the error and its derivative, obtained by comparing the reference and the measured output, are evaluated in the fuzzy interference system. By this way, the scaling factors of the proportional, integral, and derivative gains at each sampling period are updated accordingly. In view of the above critics, the contributions of this study are as follows:

(1) The number of SMC based studies for PMSG-WECS is not plentiful, mostly, direct MC topologies or conventional back-to-back converter topologies with a real DC link having an energy storage element is much more common in WECS. With this respect, this study aims to design a controller for SMC based PMSG-WECS.

(2) To the best of the authors' knowledge, FOPID controller with Mamdani fuzzy logic has been used for the first time to control a SMC based PMSG-WECS.

The paper organization is handled with seven sections. After the introduction section, a brief overview of MC topologies is given in Section 2. The mathematical models of both PMSG and SMC are given in Section 3. Section 4 overviews FO calculus. The design details of fuzzy-FOPID controller are released in Section 5. The results of the simulated cases as well as the related discussions are presented in Section 6. Lastly, the overall conclusions obtained from this work are commented in Section 7.

2. Matrix Converter Topologies

MC is a power electronic-based solution that is able to perform AC-AC power conversion without any energy storage device as well as input power factor control independently of the load. Figure 1 shows the general switch arrangement of a three-phase to three-phase MC. It consists of nine bidirectional semiconductor switches that connects the input and output stages. The desired magnitude and frequency of the output voltage are attained by applying a proper switching modulation scheme.

The MC topology was first mentioned by Venturini who was also the first to introduce this name for this converter type [32]. Later on, Venturini and Alesina introduced low frequency modulation matrix, also known as direct transfer function approach in which the output voltage is obtained by multiplying the modulation matrix by the input voltage [33]. MC topology is categorized into two forms: direct and indirect MC topology. Figure 2 shows the classification of three-phase AC-AC converters [34].

Conventional or direct MC (DMC) has a single stage with nine bidirectional switches (controlled semiconductor switch with antiparallel connected diode) distributed into four quadrants. On the other hand, indirect MC (IMC) topology has both rectifier and inverter stages. Between these stages, there is a fictitious DC link without any storage element, such as capacitor or inductor. The IMC arrangement minimizes the number of semiconductor switches being

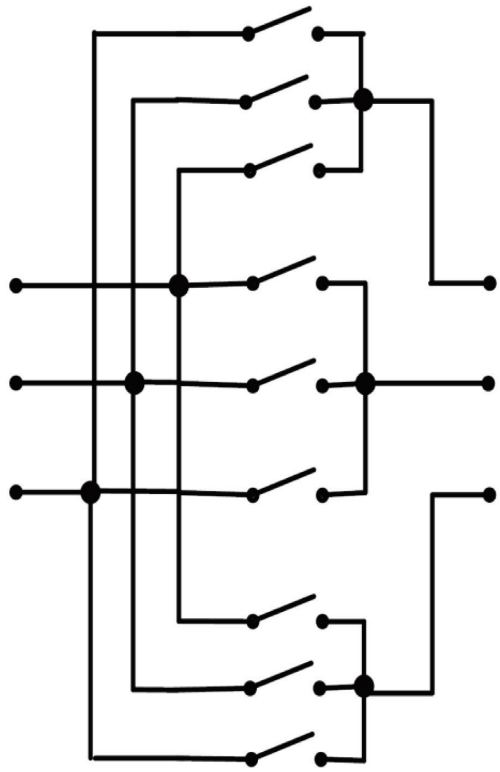

Figure 1: The general switch arrangement of MC.

utilized, developed by Kolar et al. [35]. Generally, IMC has advantages over DMC, hence this topology has gained much interest in recent years. Several topologies for IMC have been developed, including SMC family which is one of the latest arrangements proposed in the MC field. The SMC topology has some subtypes, such as very sparse MC (VSMC), ultrasparse MC (USMC), and inverting link MC (ILMC).

3. System Components

3.1. PMSG Model. Permanent magnets are used in synchronous machines due to the lack of field windings, slip rings, excitation system, and gearbox. These missing subsystems and components give PMSG many advantages over doubly fed induction generator (DFIG) such as, small size, high-power density, high reliability, and robust operation. PMSGs can be both utilized in offshore and onshore applications. PMSG requires less maintenance in offshore WECS applications compared to DFIG [14,36]. The dq voltage equations of PMSG can be written as follows: [37]

$$\begin{aligned}\frac{\mathrm{d}}{\mathrm{d}t}i_d &= \frac{1}{L_d}v_d - \frac{R}{L_d}i_d + \frac{L_q}{L_d}pw_r i_q,\\ \frac{\mathrm{d}}{\mathrm{d}t}i_q &= \frac{1}{L_q}v_q - \frac{R}{L_q}i_q + \frac{L_q}{L_q}pw_r i_q - \frac{\lambda pw_r}{L_q},\end{aligned} \tag{1}$$

where d-axis and q-axis components of the voltage terms are described as v_d and v_q, L_d and L_q are the d-axis and q-axis inductances of the PMSG, respectively, i_d and i_q are the d-axis and q-axis current components, respectively, λ is the stator flux linkage, and w_r is the angular velocity of rotor. On the other hand, R is the stator winding resistance, p is the pole count on the machine. The PMSG generates an electromagnetic torque that can be formulated as follows:

$$T_e = 1.5\rho\left[\lambda i_q + \left(L_d - L_q\right)i_d i_q\right], \tag{2}$$

where p is the number of pole pairs. The rotor speed w_r is expressed as follows:

$$\frac{\mathrm{d}}{\mathrm{d}t}w_r = \frac{1}{J}\left(T_e - Fw_r - T_m\right), \tag{3}$$

where J is the rotor inertia and F is the rotor friction. Table 1 shows the PMSG parameters used in the design.

3.2. SMC Model. SMC topology is an indirect MC topology, also known as "double stage topology", which was developed in the early 2000s [38]. SMC topology can be designed either as single- or three-phase arrangement. Figure 3 depicts the power circuit of a three-phase SMC. The rectifier stage consists of a four-quadrant current source rectifier that converts AC input voltage into DC form. In this stage, each bidirectional switch is the combination of two power semiconductor devices (IGBT, IGCT, or MOSFET) with an antiparallel diode connection. These switches can be operated either in common-emitter or common collector configuration. The inverter side is a two-level voltage source inverter, which consists of power semiconductor devices such as IGTB, IGCT, or MOSFET. The inverter is fed from a fictitious DC link without any storage element such as capacitor or inductor. The output voltage of the inverter is controlled in terms of magnitude, phase angle, and frequency. In SMC, the phase angle of the input current can also be controlled regardless of the load. With this property, unity power factor operation can be established at the SMC input. Equation (4) shows the connection matrix of the rectifier stage $S_$rec, where $S_$x represents the state of each power electronic switch available at the phase-x. When the power semiconductor element is turned on, S becomes 1 (or logic-1), on the other hand, when the power semiconductor element is turned off, S becomes zero (or logic-0). The notation S^' denotes the reciprocal state of the respected switch. In the time of switching for both cells, one switch is always closed. The necessary conditions for the switches in the rectifier stage are expressed in equation (5). The voltage and current relations that represent the rectifier operation of the indirect MC are expressed in equations (6) and (7), respectively. In Figure 3, v_p and v_0 represent the voltage of the two points represented in Figure 3, respectively. The phase input currents are represented as i_A, i_B, and i_c. At the input side, the phase voltages are denoted as v_A, v_B, and v_c. The DC current that flows from the rectifier stage to the inverter stage of the three-phase SMC is denoted by $i_$dc, as shown in Figure 3. Equation (8) shows the connection matrix of the inverter stage of the indirect MC. The necessary conditions for the power electronic switches in the inverter stage of the three-phase SMC are presented in equation (9). Equations (10) and (11) express the voltage and current

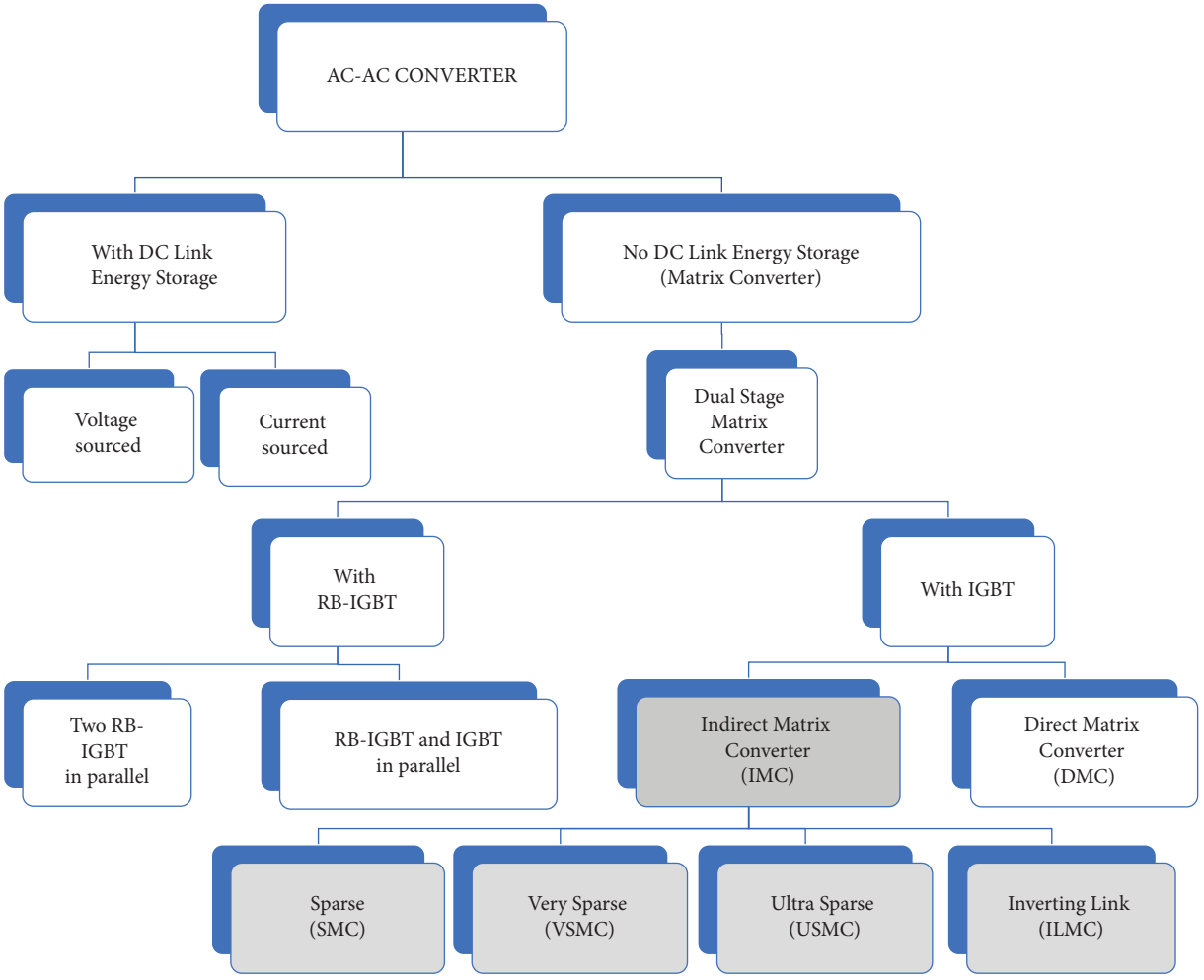

Figure 2: The classification of three-phase AC-AC converters (RB: reverse blocking) [34].

Table 1: The design parameters of the PMSG used in this work.

Parameter name	Parameter value
Rating	1.5 MW
Stator phase resistance	6 mΩ
Armature inductance	395 μH
Flux linkage	1.51 Wb-turns
Number of poles pairs	48

relations representing the inverter operation of the indirect MC, respectively. The matrix $[S_{DE}]$ expressed in equation (12) is the connection matrix of the indirect MC, which is resulted from the multiplication of the connection matrices of the rectifier and inverter stages. The semiconductor parameters used in the designing of the rectifier and inverter stages are represented in Table 2.

$$[S_{\text{rec}}] = \begin{bmatrix} S_A & S_B & S_C \\ S_A' & S_B' & S_C' \end{bmatrix}, \tag{4}$$

$$\begin{aligned} S_A \&9; + S_B + S_C &= 1, \\ S_A' \&9; + S_B' + S_C' &= 1, \end{aligned} \tag{5}$$

$$\begin{bmatrix} v_p \\ v_o \end{bmatrix} = [S_{\text{rect}}] \begin{bmatrix} v_A \\ v_B \\ v_C \end{bmatrix}, \tag{6}$$

$$\begin{bmatrix} i_A \\ i_B \\ i_c \end{bmatrix} = [S_{\text{rect}}]^T \begin{bmatrix} i_{\text{dc}} \\ -i_{\text{dc}} \end{bmatrix}, \tag{7}$$

$$[S_{\text{inv}}] = \begin{bmatrix} S_a & S_a' \\ S_b & S_b' \\ S_c & S_c' \end{bmatrix}, \tag{8}$$

$$\begin{Bmatrix} S_a + S_a' = 1, \\ S_b + S_b' = 1, \\ S_c + S_c' = 1, \end{Bmatrix} \tag{9}$$

$$\begin{bmatrix} v_a \\ v_b \\ v_c \end{bmatrix} = [S_{\text{inv}}] \begin{bmatrix} v_p \\ v_o \end{bmatrix}, \tag{10}$$

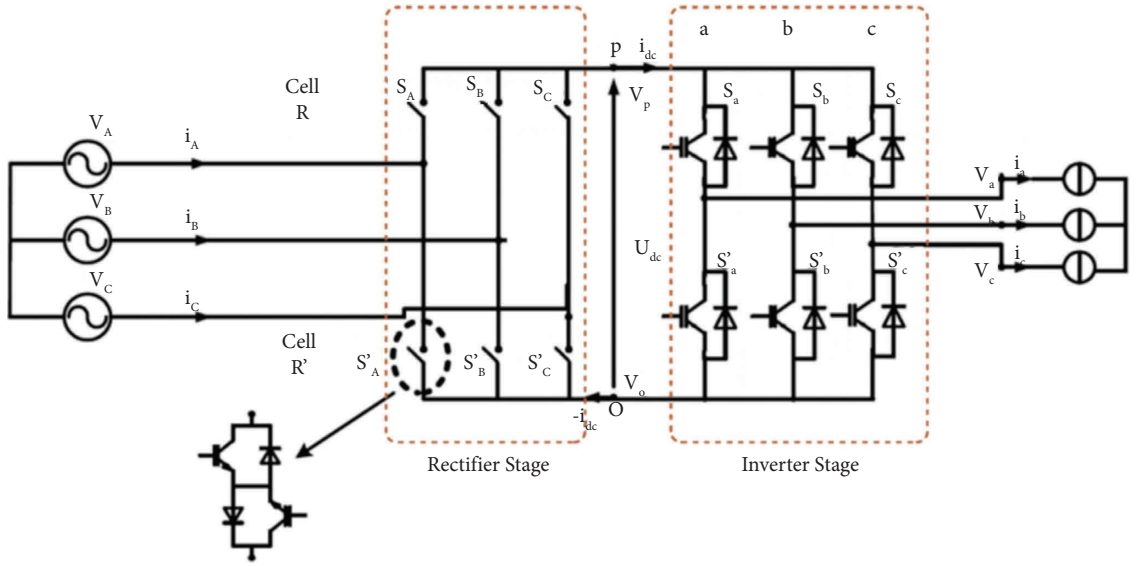

Figure 3: The power circuit of a three-phase SMC.

Table 2: The parameters of IGBT and diode used in rectifier and inverter stages.

Parameter name	IGBT	Diode
Turn on resistance	1 mΩ	1 mΩ
Turn on inductance	Ignored	Ignored
Forward voltage drop	1.0 V	0.8 V
The resistance of snubber	100 KΩ	500 Ω
The capacitance of snubber	Large	250 nF

$$\begin{bmatrix} i_{\mathrm{dc}} \\ -i_{\mathrm{dc}} \end{bmatrix} = [S_{\mathrm{inv}}]^T \begin{bmatrix} i_a \\ i_b \\ i_c \end{bmatrix}, \tag{11}$$

$$\begin{aligned} [S_{DE}] &= [S_{\mathrm{inv}}] \cdot [S_{\mathrm{rec}}] = \begin{bmatrix} S_a & S'_a \\ S_b & S'_b \\ S_c & S'_c \end{bmatrix} \cdot \begin{bmatrix} S_A & S_B & S_C \\ S'_A & S'_B & S'_C \end{bmatrix} \\ [S_{DE}] &= \begin{bmatrix} S_{Aa} & S_{Ba} & S_{Ca} \\ S_{Ab} & S_{Bb} & S_{Cb} \\ S_{Ac} & S_{Bc} & S_{Cc} \end{bmatrix}. \end{aligned} \tag{12}$$

The switching signals for the rectifier stage of the SMC are generated using sinusoidal pulse width modulation (SPWM) scheme, as shown in Figure 4. The switching signals ($S1$–$S9$) of the IGBTs are generated by making a comparison between a reference sinusoidal signal and a high frequency triangular carrier waveform. In this work, the frequency of the carrier waveform is chosen as 50 kHz for each phase. The rectifier stage is controlled in an open-loop fashion in which no feedback signals are used. Since, it is aimed to obtain the maximum value of a fictitious DC voltage from the rectifier stage. On the contrary, the SMC inverter stage is operated in a closed-loop manner so as to regulate the real power and reactive power injections at their reference values. These power injections are measured at the output of the SMC inverter stage of the three-phase SMC. The gain and the amplitude of rectifier stage is designed as 0.5 and 1, respectively. Table 3 shows the time values of the repeating sequence to generate high frequency triangular carrier waveform for the rectifier stage.

Figure 5 shows the switching signal generation for SMC inverter stage using SPWM. The switching signals ($S10$–$S15$) of the IGBTs in the inverter stage are generated by making a comparison between a reference sinusoidal signal and a high frequency triangular carrier waveform. In this work, the frequency of the carrier waveform is chosen as 25 kHz for each phase. The pulse width modulation signals are generated using the output of the FFOPID controller. The gain and the amplitude of inverter stage is designed as 1 and 3, respectively. The frequency of the carrier signal is set to 25 kHz. Table 4 shows the time values of the repeating sequence to generate high frequency triangular carrier waveform for the inverter stage.

3.3. WECS Model. Figure 6 represents the general model of the SMC based WECS including power circuits and controllers. The model contains several stages. The power generation stage consists of a wind turbine and a PMSG. This stage includes two controllers. The pitch angle controller achieves maximum utilization of wind energy, on the other hand, the operational control scheme protects the generator from very high wind speeds. Figure 7 shows the operational control scheme of the WECS. The maximum amount of energy that can be captured from the wind can be collected by performing pitch angle control. In this control, the inclination angle of the turbine blades is manipulated to capture the maximum kinetic energy from the wind. At the same time, the operational control scheme protects the generator when the wind speed exceeds a predefined reference. It relies on an algorithm that includes the maximum and minimum wind speeds. When the shaft speed exceeds the specified value, the switch is turned to zero to ensure the protection of the generator. In the normal position, the switch is connected

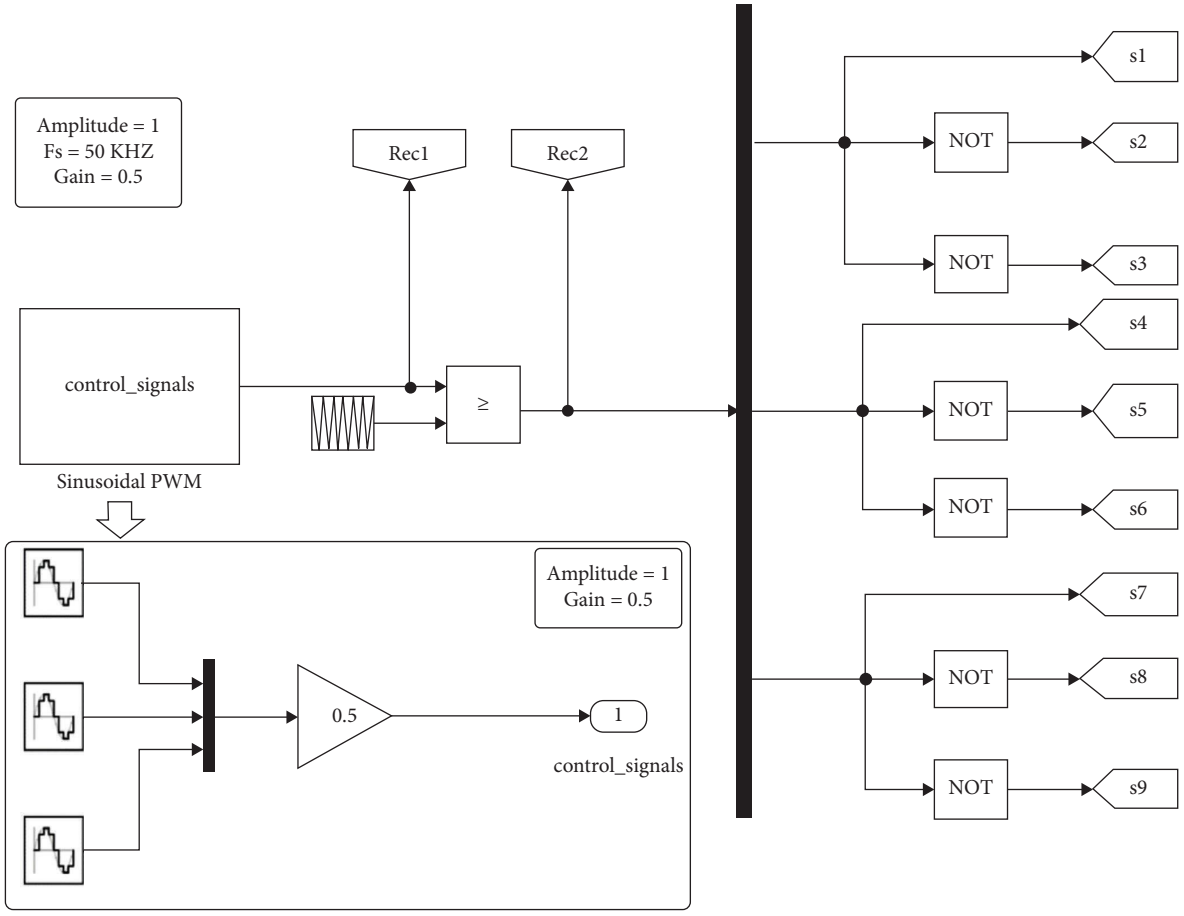

Figure 4: Switching signal generation for SMC rectifier stage.

Table 3: Repeating sequence data to generate triangular carrier waveform for rectifier stage.

Time (s)	0	0.25/50*e*3	0.5/50*e*3	0.75/50*e*3	1/50*e*3
Output	1	0	1	0	1

directly to the shaft, which connects to the turbine. The SMC is available in the second stage in which the PMSG output is connected to the rectifier stage of the SMC. The converter stage has two control schemes for each stage of the SMC, respectively. The SPWM scheme produces the required switching signals for the bidirectional switches in the rectifier stage. The inverter stage of the three-phase SMC is controlled by a FFOPID controller. This controller is the main controller of the system and more details will be given in the next sections. An LCL filter is inserted between the output of the three-phase SMC and the main power grid. This filter is used to reduce the switching harmonics of the SMC, hence the waveform distortion at the SMC output can be diminished efficiently. The reasons of selecting an LCL filter over L filter or LC filter can be justified by checking the literature. The usage of small components such as inductor and capacitor greatly reduces the filter size as well as the cost in real applications. Moreover, the high-frequency characteristics of LCL filter is −60 dB/dec, which is better than its counterparts. The LCL filter parameters used in this work are presented in Table 5. The LCL filter parameters are determined by considering the electrical parameters of the system. These parameters are the frequency and the rms value of the fundamental component of the line-to-line grid voltage, the real power as well as current rating of the inverter stage of the three-phase SMC, and the hypothetical DC link voltage of the three-phase SMC. Moreover, the switching frequency of the inverter stage of the three-phase SMC is another factor when designing the LCL filter, taking into account the values of the inductance of the transformer and the inductance of the semiconductors of the SMC Inverter stage.

The designed WECS should provide the necessary amount of real power generation and reactive power generation/absorption to the main electrical grid. Since, no storage element is used between rectifier and inverter stages, the converted power from the wind is first converted into DC power in the fictitious DC link, and then converted back into AC power which is injected into the grid. The designed FFOPID controller simultaneously regulates the real and reactive power injections into the grid. By this way, unity power factor operation of the WECS can be ensured while the injected active power is controlled independently.

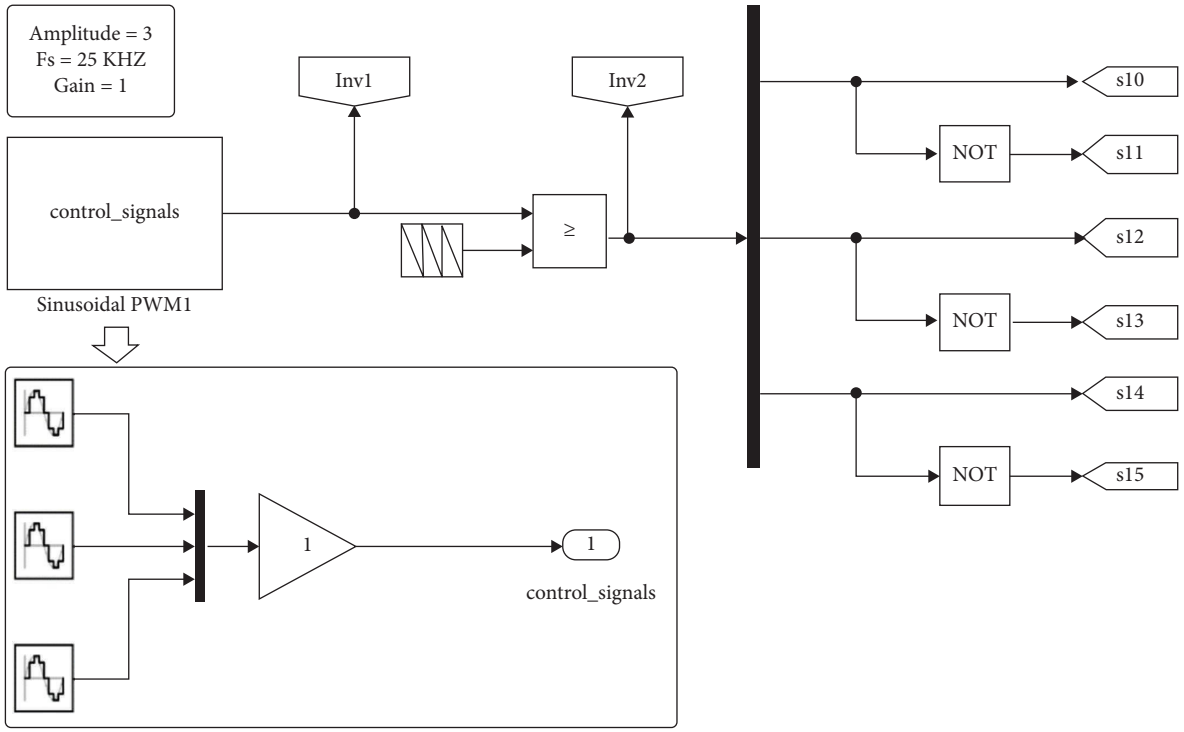

Figure 5: Switching signal generation for SMC inverter stage.

Table 4: Repeating sequence data to generate triangular carrier waveform for inverter stage.

Time (s)	0	0.25/50*e*3
Output	1	0

4. Overview of Fractional Order Calculus

The lack of a simple geometric explanation and the solution for FO differential equations have motivated to develop calculus to solve complex problems. FO calculus is a branch of mathematics science in which performing the differentiation and integration operations under an arbitrary order are possible [39]. This order by definition may be a real or complex number. FO calculus relates to fractional dimension infinite memory and chaotic behavior. FO has found many application areas such as astronomy, control problems, and industrialization problems [40,41]. FO is found to be fulfilled of articulating marvels owning long-range memory uncommon impacts that are challenging to handle through classical integer-order calculus. With the increment of inquire about in this field, expanding concentration has been watched within the alteration of fragmentary calculus as a fruitful modeling contraption for complicated frameworks that gives impulse to development in dynamical examination and direction. Fragmentary calculus shows up to be conceivably contender to consolidate bigger models through segregating agile subordinate on the clarification of involvedness [42]. Incorporating FO calculus into control strategies is shown to improve the control system performance and robustness with less control effort [43,44]. FO differentiator can be represented as a persistent differential integral operator [45–47],

$$aD_t^{\gamma} = \begin{cases} \dfrac{\mathrm{d}^{\gamma}}{\mathrm{d}t^{\gamma}}, & \Re(\gamma) > 0, \\ 1, & \Re(\gamma) = 0, \\ \displaystyle\int_a^t (\mathrm{d}\tau)^{-\gamma}, & \Re(\gamma) < 0. \end{cases} \tag{13}$$

In equation (13), γ is the differentiation order, and a is a constant that can be identified by the initial conditions of the given problem. A number of common definitions is available for FO calculus. The Riemann-Liouville and Caputo definitions are represented as follows: [48]

$$aD_t^{\gamma} f(t) = \frac{1}{\Gamma(n-1)} \frac{\mathrm{d}^n}{\mathrm{d}t^n} \int_a^t \frac{f(\tau)}{f(t-\tau)^{\gamma-n+1}} \mathrm{d}\tau, \tag{14}$$

where n is the derivative order that describes the lowest and highest limits of γ, explained by this expression $n-1 < \gamma < n$. The ordinary gamma function $\Gamma(\gamma)$ used in equation (14) can be detailed as follows:

$$\Gamma(\gamma) = \int_0^{\infty} e^{-u} u^{\gamma-1} \mathrm{d}u, \quad \Re(\gamma) > 0. \tag{15}$$

The Grunwald-Letnikov definitions used in this study are represented as follows:

$$aD_{\gamma}^t f(t) = \lim_{h \longrightarrow 0} h^{-\gamma} \sum_{j=0}^{[(t-a)/h]} (-1)^j \binom{\gamma}{j} f(t-jh), \tag{16}$$

where h is the time increment. The binomial coefficient is given as follows:

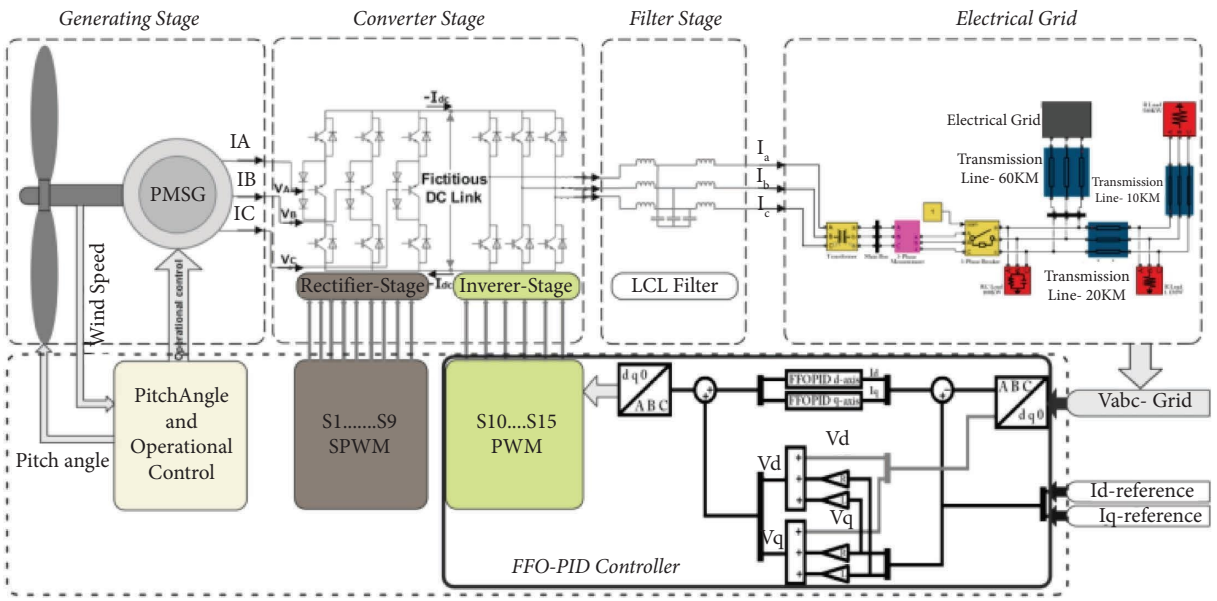

Figure 6: The general model of the SMC based WECS.

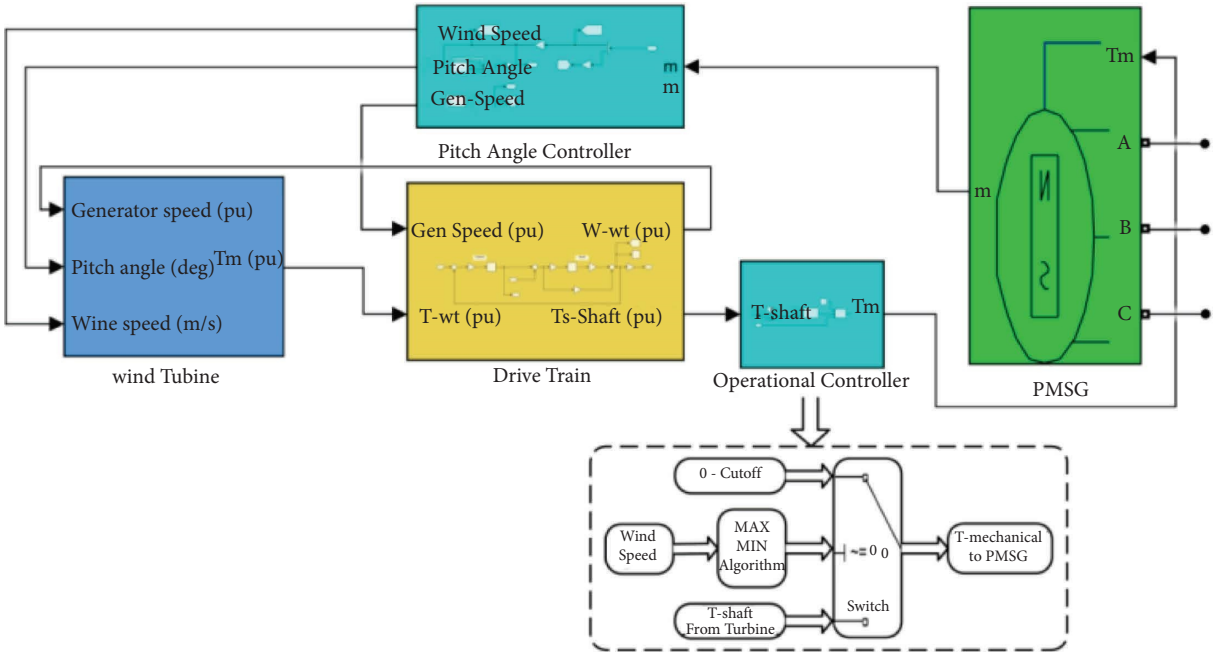

Figure 7: The operational control scheme of the WECS.

Table 5: LCL filter parameters used in the design.

Parameter name	Parameter value
SMC side inductor	0.6 mH
Grid side inductor	51 mH
Capacitor	22 μF

$$\binom{\gamma}{j} = \frac{\gamma!}{j!(\gamma - j)!} = \frac{\Gamma(\gamma + j)}{\Gamma(\gamma + 1)\Gamma(\gamma - j + 1)}. \quad (17)$$

When a fractional order differential equation is considered, equation (16) can be effectively used to find a numerical solution of the given problem [49].

5. Fuzzy FOPID Controller Design

The application of FO calculus to energetic systems began in 1960 [50]. Since at that point, the investigation on FO based control approaches have been expanded to different research areas in engineering science. For an illustration, a FO based PID (FOPID) controller may be a combination of a classical PID control scheme and a group of FOs. The dynamics of a FOPID controller can be represented as a transfer function as follows:

$$G_c(s) = K_P + K_I s^{-\lambda} + K_D s^{\mu}. \quad (18)$$

In equation (18), the gains of classical PID controller are denoted as *K_P*, *K_I*, and *K_D*, respectively. *K_P* is the proportional gain, *K_I* is the integral gain, and *K_D* is the derivative gain. The fractional term of the integrator section of the PID controller is λ, while the fractional term of the derivative section of the PID controller is μ. The output of the FOPID controller expressed in time-domain can be shown as follows:

$$\text{Output}(t) = K_P e(t) + K_I D^{-\lambda} e(t) + K_D D^{\mu} e(t). \quad (19)$$

It is clear that, within the FOPID controller, separated from the normally considered three parameters such as *K_P*, *K_I,* and *K_D*, two additional control parameters such as (λ, μ) are also experienced. Thus, in the FOPID controller design stage, a total of five parameters can be effectively considered. By this way, five nonlinear equations with five unknowns can be solved in a straight manner. In this work, the FOPID controller design is carried out by using the available FOMCON toolbox [51,52]. Fuzzy logic works using linguistic notation, as it gives flexibility in expressions with an easy language, helps to solve complex uncertain problems in real problems. For example, a fuzzy logic supported controller can be considered for the systems having nonlinearity and uncertainty between inputs and outputs. As in case of a classical PID controller, since the gains are fixed, the required performance may not be met in most times when the controlled system is nonlinear and complex. Consequently, modifying the gains of a FOPID controller dynamically can lead to improved control performance, even though when there is a variation in load and/or external disturbances. In view of this aspect, a Mamdani type fuzzy logic concept is combined with the FOPID controller in this work. This type of control approach is recently proposed in many works [53–55]. The fuzzy-FOPID (FFOPID) controller could be a bunch of fuzzy-based rules connected in collection with PID control activity. In this control approach, the fuzzy-based rules are outlined to utilize the system error and the error of the derivative to tune the scaling factors of the PID controller parameters, such as proportional, integral, and derivative terms. Utilizing these scaling variables, the controller gains are upgraded at each sampling period. Figure 8 depicts the block diagram of the FFOPID controller used in this work. The d*q*-axis current components measured at SMC output are used as reference to control the d*q*-axis currents at SMC output, to regulate the injected real and reactive power from WECS into the grid.

The FFOPID controller gains are calculated as follows:

$$\left\{ \begin{array}{l} K_P = K_P + \Delta K_P, \\ K_I = K_I + \Delta K_I, \\ K_D = K_D + \Delta K_D, \end{array} \right\}, \quad (20)$$

where *K_P*, *K_I*, and *K_D* are the initial gains, and ΔK_P, $[\![\Delta K]\!]\_I$, and ΔK_D are the dynamic scaling factors computed by fuzzy based rules. In this work, a Mamdani type interference system is connected to the FFOPID controller with two triangle membership functions for the input stage of the controller. On the other hand, a total of three Gaussian membership functions for the controller outputs are utilized. Two separate FFOPID controllers are designed for each axis component of the output current of the three-phase SMC after coordinate transformation. Figure 9 shows the overall closed-loop control scheme of the PMSG based WECS. The settled parameters of the FFOPID controller are listed in Table 6.

The rule base is the significant portion of the fuzzy interference system design. Based on the current input, the input and output linguistic variables are related by this rule base. Tables 7–9 shows fuzzy linguistic rules for ΔK_P, $[\![\Delta K]\!]\_I$, and ΔK_D for each d*q*-axis FFOPID controller, respectively. The membership functions used in this work are designated with some linguistic variables. Namely, for the input side, seven different linguistic variables are planned. These are as follows: negative big (NB), negative medium (NM), negative small (NS), zero (Z), positive small (PS), positive medium (PM), and positive big (PM), respectively. For the output side, two different linguistic variables are planned such as (Small) and (Big), respectively. Figures 10 and 11 presents the input fuzzy membership functions, respectively. These functions are designed for error and change-in-error signals obtained at the input, respectively. On the other hand, the output fuzzy membership functions are denoted in Figure 12. The output surfaces of the designed fuzzy inference system are illustrated graphically in Figures 13–15. These surfaces signify the relationship between inputs and output as 3D surface view and specify how the scaling factor could vary based on the magnitude of input error and change-in-error. As seen, the scaling factors are set bigger for the larger amplitude of error and change-in-error, while these values are gradually reduced for smaller error and change-in-error values. To determine the crisp output, the center of gravity is used for defuzzification.

6. Simulation Results and Discussion

The closed-loop dynamic performance of the FFOPID controller is verified under fixed wind speed of 9 m/s when step changes are applied to *dq*-axis current references. Moreover, a comparison with classical PID controller is also made in this section. Figures 16 and 17 illustrates three-phase output voltage and current waveforms of the PMSG recorded at the input of the SMC, respectively. Although the voltage waveforms do not contain any harmonics, since no filter is used at the SMC input, the current waveforms contain switching noise and harmonics due to the rectifier switching. On the other hand, Figures 18 and 19 shows three-phase output voltage and current waveforms of the SMC after LCL filter, respectively. It is clearly observed that the LCL filter reduces the switching noise as well as harmonics in both waveforms. The voltage and current waveforms of the fictitious DC link of the SMC are presented in Figures 20 and 21, respectively. As seen, the DC-link voltage obtained greater than 800 V that has a ripple factor of around 6.75%. To quantitatively express the harmonic content of the voltage and current waveforms, THD measurements are also carried out in the simulation

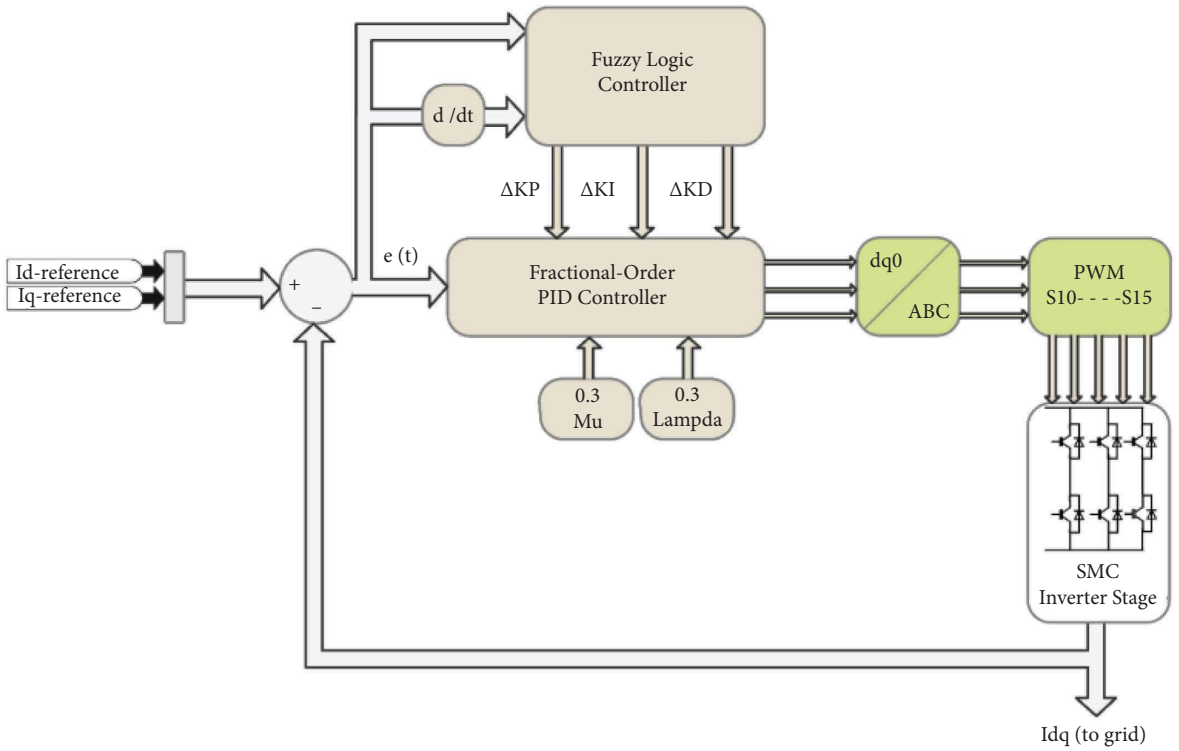

Figure 8: Block diagram of the FFOPID controller.

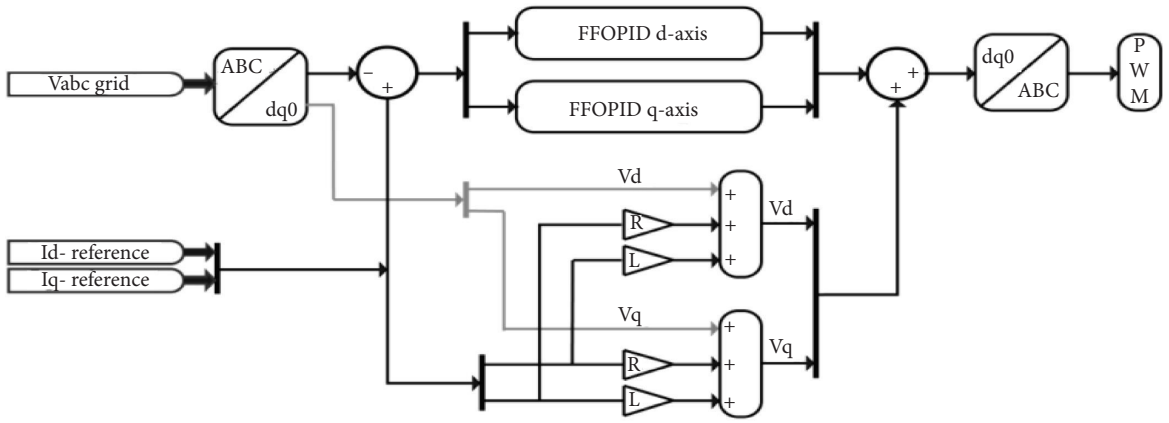

Figure 9: The overall closed-loop control scheme of the PMSG based WECS.

Table 6: Fixed parameters of the FFOPID controller.

K_P	K_I	K_D	γ	μ
1.2	0.25	0.01	0.3	0.3

studies. THD measurements before the LCL filter indicate a THD of 0.83% for the SMC output voltage, while a THD of 0.2% for the SMC output current. Measurement after the LCL filter indicates better results. THD of SMC output voltage is reduced to 0.08%, while the THD of the SMC output current is reduced to 0.1% by using the LCL filter. The FFOPID controller response and its comparison with the classical PID controller response are represented in Figures 21 and 22, respectively. In each comparison study, when Id is kept constant Iq is applied a step-change and vice versa. In the first case, the constant Id value (Id = 0.8 pu) is chosen with a step-change in Iq (+0.1 pu to −0.2 pu) is applied, as shown in Figure 22. In the second case, the constant Iq value (Iq = 0.0 pu) is chosen with a step-change in Id (+0.8 pu to +0.6 pu), as shown in Figure 23. The system that uses the classical PID controller takes a long time to reach the desired response, as well as an acceptable value of the overshot until the steady-state is reached. But, when FFOPID controller is activated, the system takes less time to reach the desired response when compared with the classical PID controller. There is no value to be mentioned for overshoot as well as access to the steady-state value is even faster. These comparisons reveal the fact that the Mamdani based fuzzy rules are able to dynamically adjust the gains of the controllers in each

Table 7: Fuzzy linguistic rule and ΔK_P output for dq-axis.

d,q		Δe						
	ΔK_P	NB	NM	NS	Z	PS	PM	PB
	NB	Big	Big	Big	Big	Big	Big	Big
	NM	Small	Big	Big	Big	Big	Big	Big
	NS	Small	Small	Big	Big	Big	Small	Small
e	Z	Small	Small	Small	Big	Small	Small	Small
	PS	Small	Small	Big	Big	Big	Small	Small
	PM	Small	Big	Big	Big	Big	Big	Small
	PB	Big	Big	Big	Big	Big	Big	Big

Table 8: Fuzzy linguistic rule and ΔK_I output for dq-axis.

d,q		Δe						
	ΔK_P	NB	NM	NS	Z	PS	PM	PB
	NB	Small	Small	Small	Small	Small	Small	Small
	NM	Big	Big	Small	Small	Small	Big	Big
	NS	Big	Big	Big	Small	Big	Big	Big
e	Z	Big	Big	Big	Big	Big	Big	Big
	PS	Big	Big	Big	Small	Big	Big	Big
	PM	Big	Big	Small	Small	Small	Big	Big
	PB	Small	Small	Small	Small	Small	Small	Small

Table 9: Fuzzy linguistic rule and ΔK_D output for dq-axis.

d,q		Δe						
	ΔK_P	NB	NM	NS	Z	PS	PM	PB
	NB	Small	Small	Small	Small	Small	Small	Small
	NM	Big	Big	Small	Small	Small	Big	Big
	NS	Big	Big	Big	Small	Big	Big	Big
e	Z	Big	Big	Big	Big	Big	Big	Big
	PS	Big	Big	Big	Small	Big	Big	Big
	PM	Big	Big	Small	Small	Small	Big	Big
	PB	Small	Small	Small	Small	Small	Small	Small

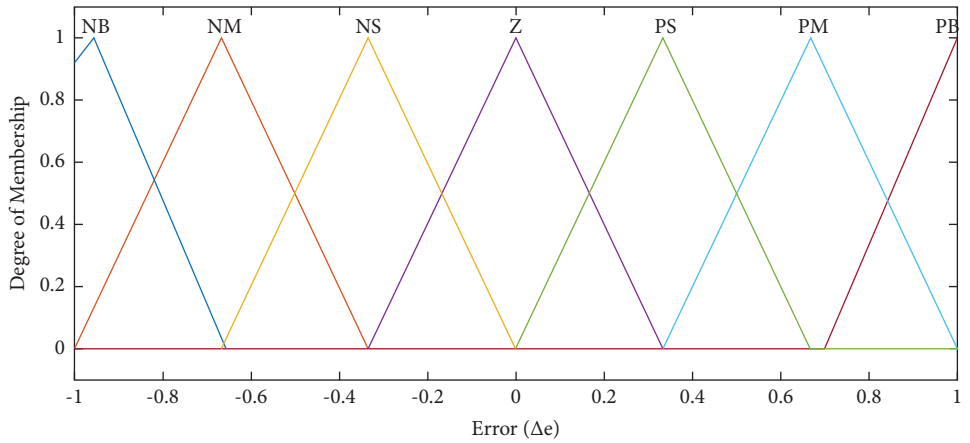

Figure 10: Input (error) for dq-axis.

sample time, while the FO part can compete with the nonlinearity of the WECS. Consequently, the FFOPID controller is more effective than fixed parameter PID controller when dynamic changes are applied to the reference current signals. A qualitative comparison of FFOPID controller and classical PID controller in terms of rise time, overshoot, settling time, and steady-state time is presented in Tables 10 and 11. The numerical results obviously clarifies the superiority of the dynamic performance of the FFOPID controller.

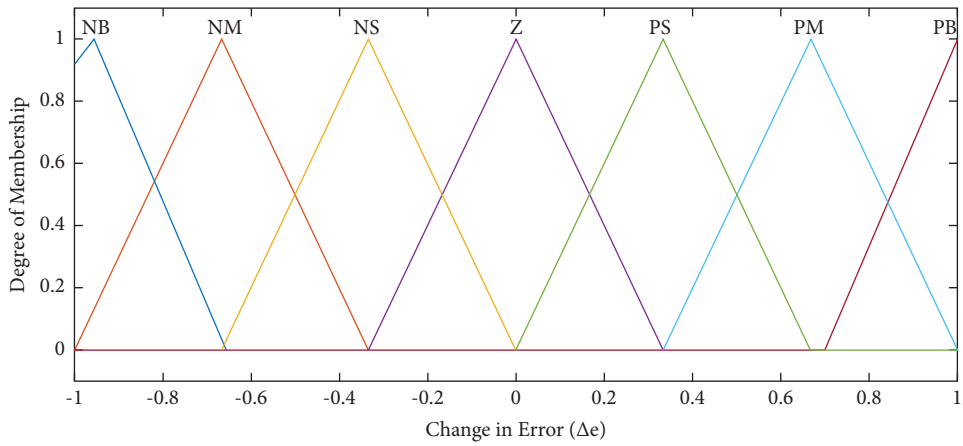

Figure 11: Input (change-in-error) for dq-axis.

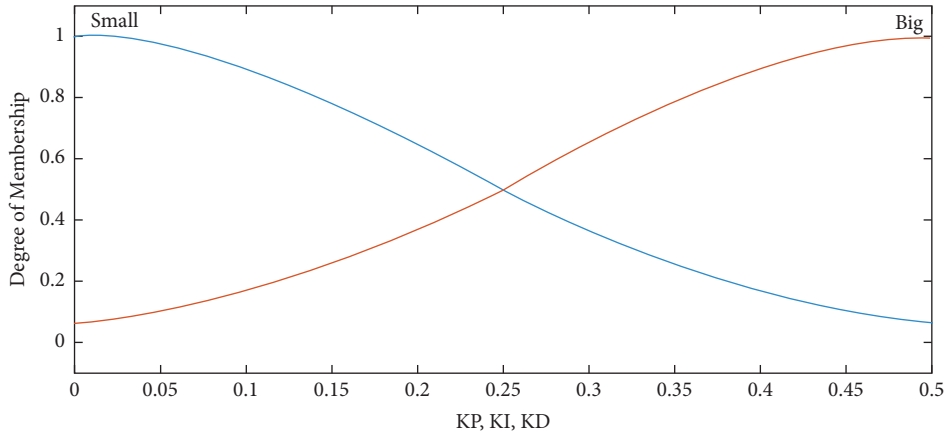

Figure 12: Outputs $\Delta K_P, \Delta K_I$, and ΔK_D for dq-axis.

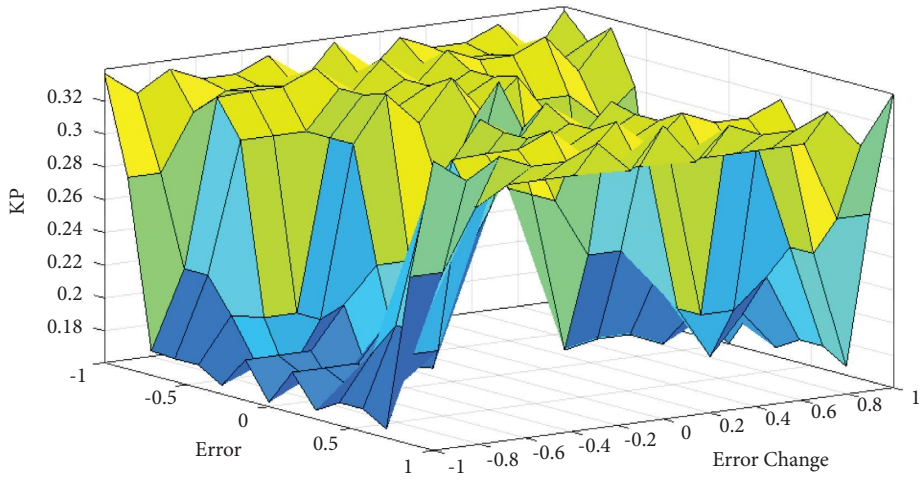

Figure 13: Outputs ΔK_P for dq-axis.

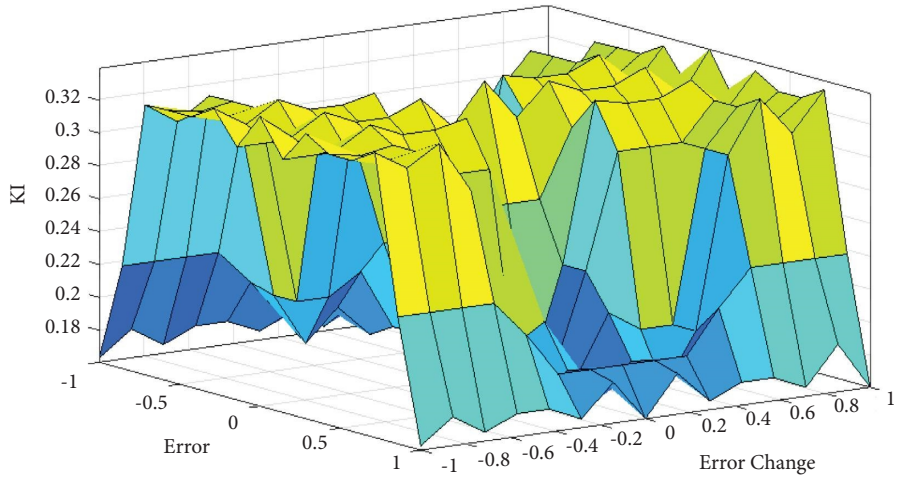

Figure 14: Outputs ΔK_I for dq-axis.

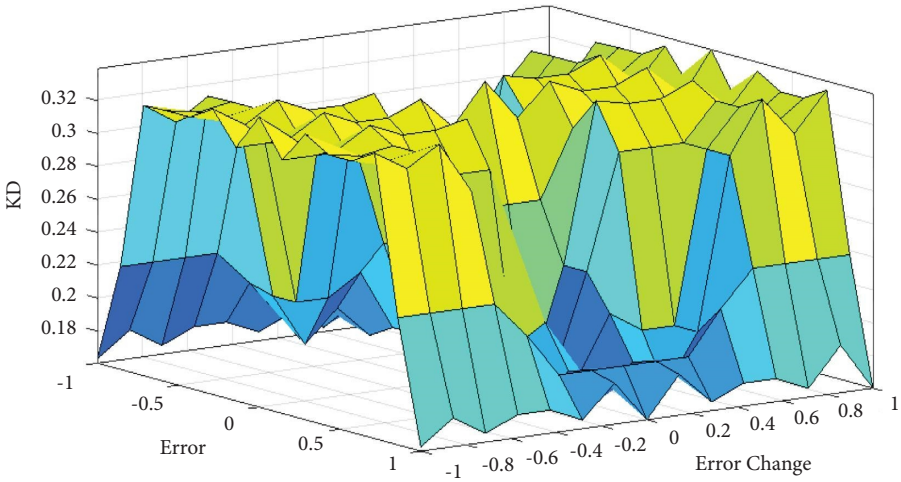

Figure 15: Outputs ΔK_D for dq-axis.

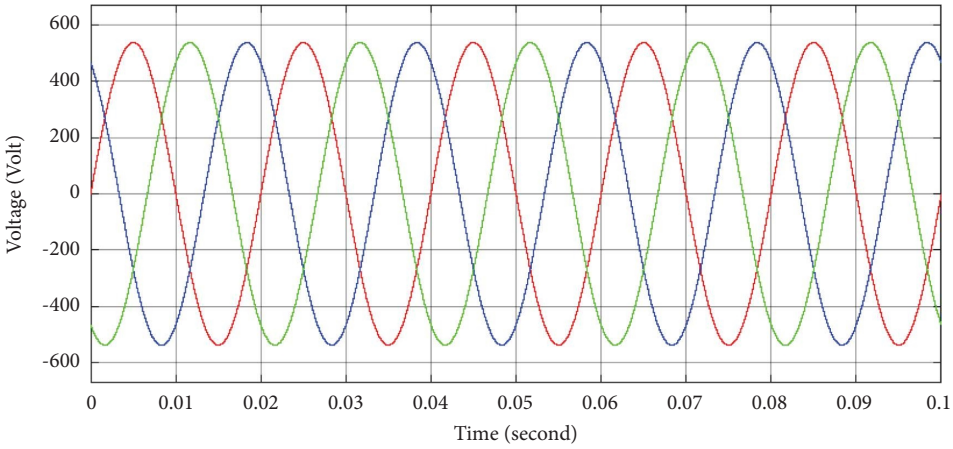

Figure 16: PMSG output voltage waveforms.

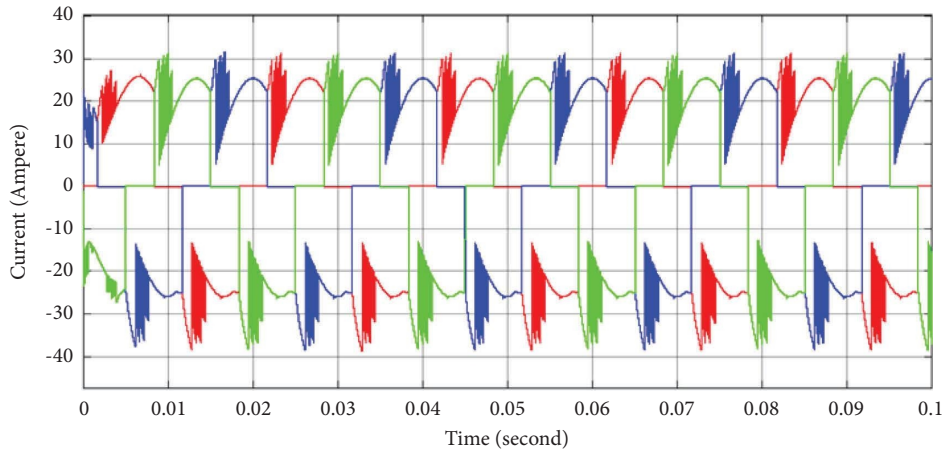

Figure 17: PMSG output current waveforms.

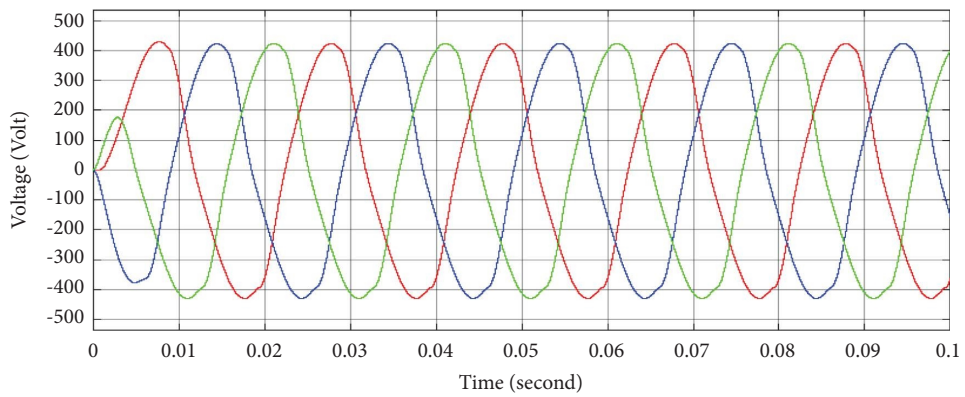

Figure 18: SMC output voltage waveforms after LCL filter.

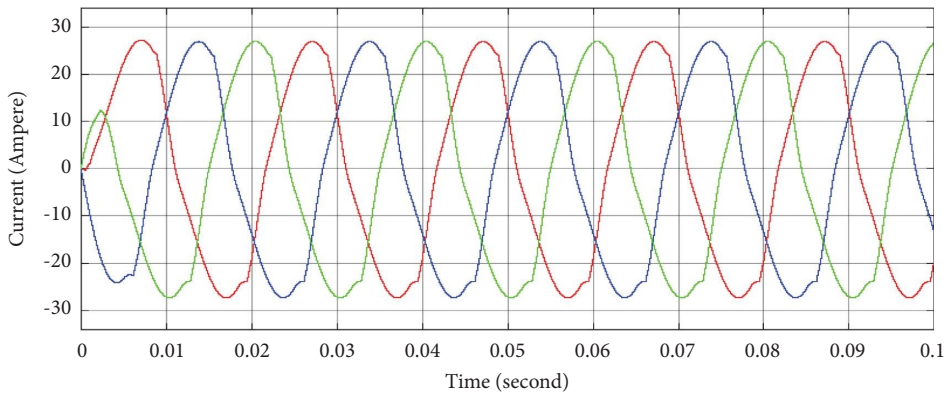

Figure 19: SMC output current waveforms after LCL filter.

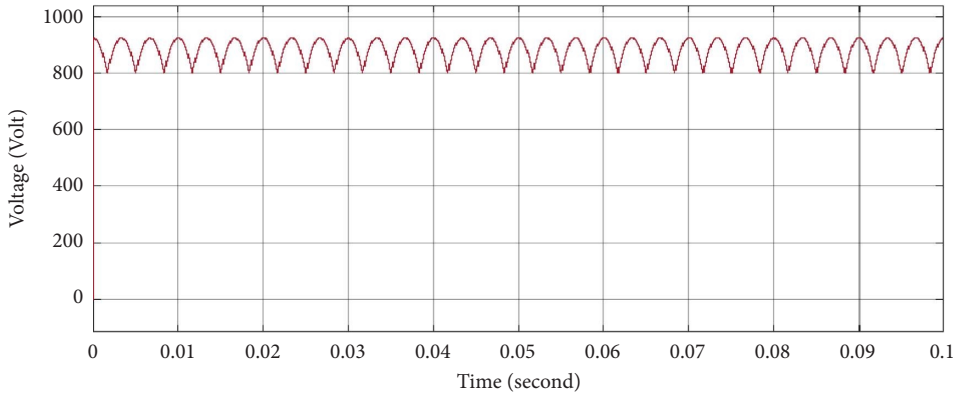

Figure 20: DC voltage waveform at rectifier stage output.

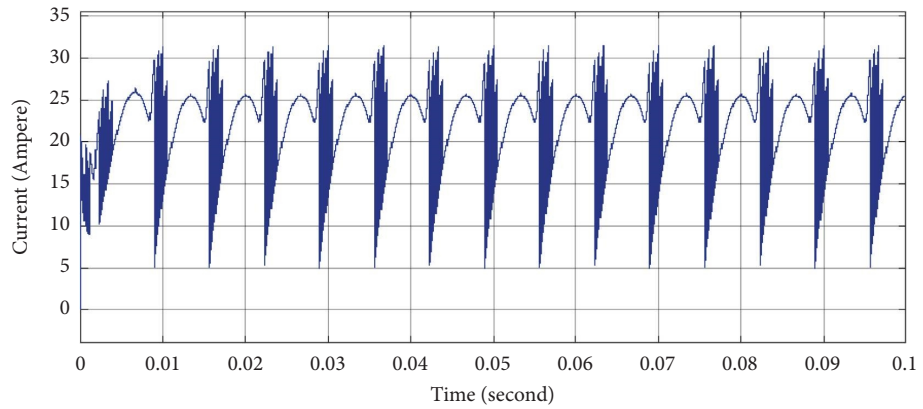

Figure 21: DC current waveform at rectifier stage output.

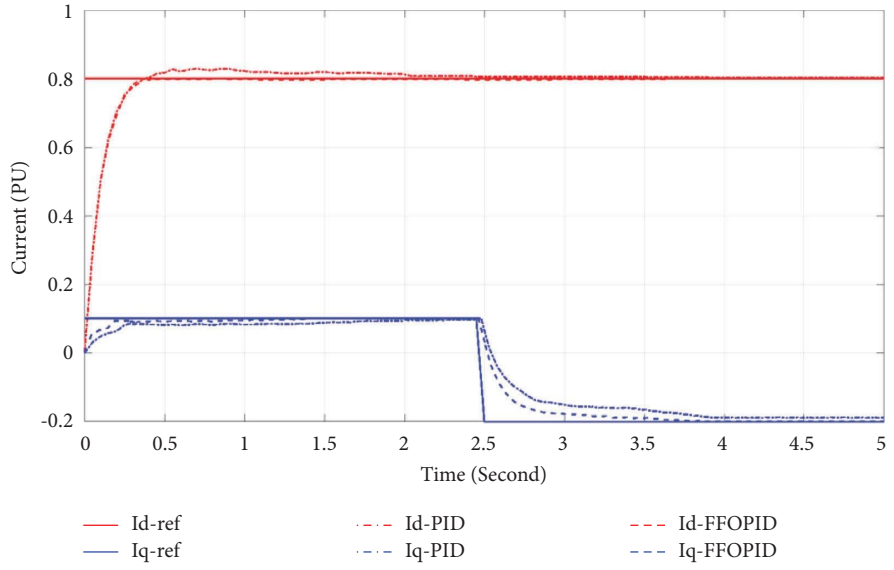

Figure 22: The FFOPID and PID response when Id is constant and Iq is changed.

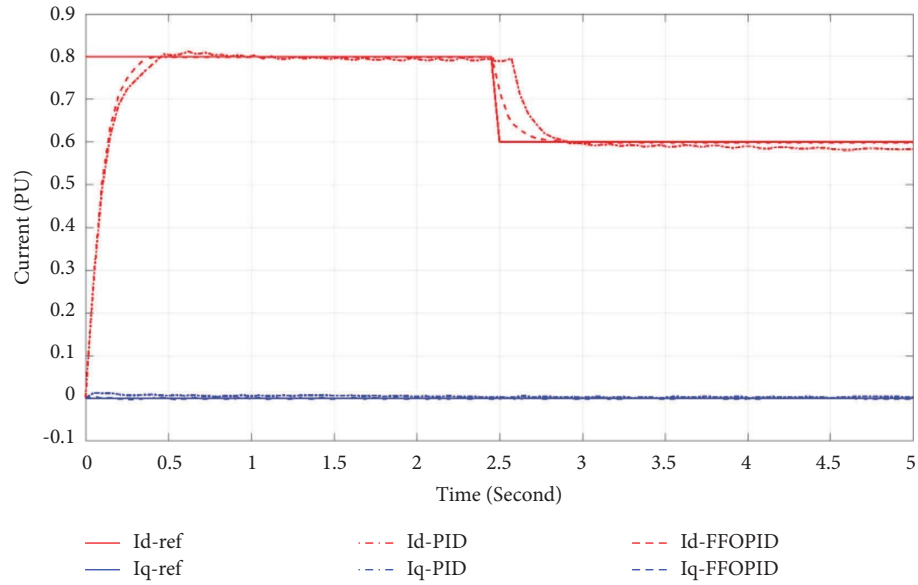

Figure 23: The FFOPID and PID response when Iq is constant and Id is changed.

Table 10: The comparison in numbers between classical PID and FFOPID when Iq is changed and Id is constant.

Iq value	Controller type	Rise time	Overshoot	Settling time	Steady-state time
+0.1	Fuzzy fractional order PID controller	0.18	0.00	0.19	0.20
	Classical PID controller	0.20	0.00	0.25	0.32
−0.2	Fuzzy fractional order PID controller	3.00	0.00	3.50	3.55
	Classical PID controller	3.50	0.00	3.80	4.00

Table 11: The comparison in numbers between classical PID and FFOPID when Id is changed and Iq is constant.

Iq value	Controller type	Rise time	Overshoot	Settling time	Steady-state time
+0.8	Fuzzy fractional order PID controller	0.30	0.00	0.40	0.48
	Classical PID controller	0.42	0.62	1.50	1.60
+0.6	Fuzzy fractional order PID controller	2.60	0.00	2.70	2.85
	Classical PID controller	2.80	3.60	2.90	3.30

7. Conclusion

Since the truth that wind power is one of the foremost vital renewable power sources in the world, wind energy conversion systems are open to be created and ceaselessly holding their notoriety. On the other hand, the erratic nature of the wind and the nonlinearity of the system components force researchers to design robust controllers for such renewable systems. Permanent magnet synchronous generators have many advantages over doubly fed induction generators and their applications are continuously rising. In this work, a fuzzy supported fractional order PID control scheme is designed and presented to effectively control a 1.5 MW rated PMSG based wind energy conversion system. This system also contains a high-power density sparse matrix converter with reduced switching elements and without any energy storage element at the DC link. The effectiveness of the proposed control approach is evaluated by performing some simulation studies. Fast dynamic performance of the proposed control system especially during step changes in the reference signals of the current axis components are observed. It is revealed that although PID controller performance is acceptable in steady-state conditions, the proposed controller has better dynamics when rise time, overshoot, settling time, as well as steady-state reaching time values are checked.

Data Availability

The datasets generated and/or analyzed during the study are available from the corresponding author upon reasonable request.

Conflicts of Interest

The authors declare that they have no conflicts of interest.

References

[1] A. Bento, G. Paraíso, P. Costa et al., "On the potential contributions of matrix converters for the future grid operation, sustainable transportation and electrical drives innovation," *Applied Sciences*, vol. 11, no. 10, p. 4597, 2021.

[2] S. Li, Z. Jin, X. Liu, X. Han, and W. Deng, "Open-current vector based SVM strategy of sparse matrix converter for

common-mode voltage reduction," *IEEE Transactions on Industrial Electronics*, vol. 68, no. 9, pp. 7757–7767, 2021.

[3] A. Ammar, H. Y. Kanaan, N. Moubayed, M. Hamouda, and K. Al-Haddad, "A review on three-phase AC/AC power converters dervied from the conventional indirect matrix converter," in *Proceedings of the IEEE International Conference on Industrial Technology*, pp. 432–437, Buenos Aires, Argentina, February 2020.

[4] D. Varajão and R. E. Araújo, "Modulation methods for direct and indirect matrix converters: a review," *Electronics*, vol. 10, no. 7, pp. 812–829, 2021.

[5] K. B. Tawfiq, A. S. Mansour, H. S. Ramadan, M. Becherif, and E. E. El-Kholy, "Wind energy conversion system topologies and converters: comparative review," *Energy Procedia*, vol. 162, pp. 38–47, 2019.

[6] K. B. Tawfiq, A. S. Mansour, M. N. Ibrahim, E. E. El-Kholy, and P. Sergeant, "Implementation of matrix converter in wind energy conversion system with modified control techniques," *Electric Power Components and Systems*, vol. 47, no. 14-15, pp. 1316–1331, 2019.

[7] S. Taraft, D. Rekioua, D. Aouzellag, and S. Bacha, "A proposed strategy for power optimization of a wind energy conversion system connected to the grid," *Energy Conversion and Management*, vol. 101, pp. 489–502, 2015.

[8] E. Agheb, N. Holtsmark, H. K. Høidalen, and M. Molinas, "High frequency wind energy conversion system for offshore DC collection grid - Part I: comparative loss evaluation," *Sustainable Energy, Grids and Networks*, vol. 5, pp. 167–176, 2016.

[9] P. Szcześniak, J. Kaniewski, and M. Jarnut, "AC-AC power electronic converters without DC energy storage: a review," *Energy Conversion and Management*, vol. 92, pp. 483–497, 2015.

[10] N. Taib, B. Metidji, and T. Rekioua, "Performance and efficiency control enhancement of wind power generation system based on DFIG using three-level sparse matrix converter," *International Journal of Electrical Power & Energy Systems*, vol. 53, pp. 287–296, 2013.

[11] M. Yuhendri, "Aslimeri "Optimum torque control of direct driven wind energy conversion systems fed sparse matrix converter"," *Journal of Electrical Systems*, vol. 14, no. 3, pp. 12–25, 2018.

[12] K. Jayanthi and N. S. Kumar, "Design of SVM technique for Matrix converter in a PMSG based wind energy conversions," *International Journal of Pure and Applied Mathematics*, vol. 120, no. 6, pp. 11017–11036, 2018.

[13] M. Yuhendri, A. Ahyanuardi, and A. Aswardi, "Direct torque control strategy of PMSM employing ultra sparse matrix converter," *International Journal of Power Electronics and Drive Systems*, vol. 9, no. 1, pp. 64–72, 2018.

[14] L. Pan and C. Shao, "Wind energy conversion systems analysis of PMSG on offshore wind turbine using improved SMC and extended state observer," *Renewable Energy*, vol. 161, pp. 149–161, 2020.

[15] M. H. Qais, H. M. Hasanien, and S. Alghuwainem, "A novel LMSRE-based adaptive PI control scheme for grid-integrated PMSG-based variable-speed wind turbine," *International Journal of Electrical Power & Energy Systems*, vol. 125, Article ID 106505, 2021.

[16] B. Herissi and D. Boudjehem, "Fractional-order fuzzy controller for a PMSG wind turbine system," *International Journal of Systems Science*, vol. 51, no. 16, pp. 3237–3250, 2020.

[17] B. Babaghorbani, M. T. Beheshti, H. A. Talebi, and A. Talebi, "A Lyapunov-based model predictive control strategy in a permanent magnet synchronous generator wind turbine," *International Journal of Electrical Power & Energy Systems*, vol. 130, Article ID 106972, 2021.

[18] M. I. Marei, A. Mohy, and A. A. El-Sattar, "An integrated control system for sparse matrix converter interfacing PMSG with the grid," *International Journal of Electrical Power & Energy Systems*, vol. 73, pp. 340–349, 2015.

[19] G. Mann, B. Hu, and R. Gosine, "Analysis and performance evaluation of linear-like fuzzy PI and PID controllers," in *Proceedings of the 6th International Fuzzy Systems Conference*, pp. 383–390, Barcelona, Spain, July 1997.

[20] I. Podlubny, "Fractional differential equations," *Volume 198 of Mathematics in Science and Engineering*, Academic Press, San Diego, CA, USA, 1999.

[21] Y. Q. Chen, I. Petráš, and D. Y. Xue, "Fractional order control-a tutorial," in *Proceedings of the American Control Conference (ACC '09)*, pp. 1397–1411, St. Louis, MO, USA, June 2009.

[22] A. Tepljakov, E. Petlenkov, and J. Belikov, "FOMCON: a MATLAB toolbox for fractional-order system identification and control," *International Journal of Microelectronics and Computer Science*, vol. 2, no. 2, pp. 51–62, 2011.

[23] A. T. Azar, S. Vaidyanathan, and A. Ouannas, *Fractional Order Control and Synchronization of Chaotic Systems*, p. 688, Springer, Berlin, Germany, 2017.

[24] N. Kanagaraj and V. N. Jha, "Design of an enhanced fractional order PID controller for a class of second-order system," *COMPEL-The International Journal for Computation and Mathematics in Electrical and Electronic Engineering*, vol. 40, no. 3, pp. 579–592, 2021.

[25] P. Khan, Y. Khan, and S. Kumar, "Activity-based tracking and stabilization of human heart rate using fuzzy FO-PID Controller," *IEEE Journal of Emerging and Selected Topics in Industrial Electronics*, vol. 3, no. 2, pp. 372–381, 2022.

[26] A. T. Azar, S. Vaidyanathan, and A. Ouannas, *Fractional Order Control and Sof Chaotic Systems"*, Springer, Berlin, Germany, 2017.

[27] S. Ahmed, "Parameter and delay estimation of fractional order models from step response," in *Proceedings of the 9th International Symposium on Advanced Control of Chemical Processes*, pp. 942–947, Whistler, British Columbia, Canada, June 2015.

[28] D. E. Rivera, M. Morari, and S. Skogestad, "Internal model control: PID controller design," *Industrial and Engineering Chemistry Process Design and Development*, vol. 25, no. 1, pp. 252–265, 1986.

[29] V. Haji Haji and C. A. Monje, "Fractional order fuzzy-PID control of a combined cycle power plant using particle swarm optimization algorithm with an improved dynamic parameters selection," *Applied Soft Computing*, vol. 58, pp. 256–264, 2017.

[30] A. Kumar and V. Kumar, "Hybridized ABC-GA optimized fractional order fuzzy pre-compensated FOPID control design for 2-DOF robot manipulator," *AEU-International Journal of Electronics and Communications*, vol. 79, pp. 219–233, 2017.

[31] M. A. George, D. V. Kamat, and C. P. Kurian, "Electronically tunable ACO based fuzzy FOPID controller for effective speed control of electric vehicle," *IEEE Access*, vol. 9, pp. 73392–73412, 2021.

[32] M. Venturini, "A new sine wave in sine wave out, conversion technique which eliminates reactive elements," *Proceedings of POWERCON*, vol. 7, pp. E3.1–E3.15, 1980.

[33] A. Alesina and M. Venturini, "Analysis and design of optimum-amplitude nine-switch direct AC-AC converters," *IEEE Transactions on Power Electronics*, vol. 4, no. 1, pp. 101–112, 1989.

[34] J. W. Kolar and T. Friedli, "Comprehensive evaluation of three-phase ac-ac PWM converter systems," in *Proceedings of the IECON 2010-36th Annual Conference on IEEE Industrial Electronics Society*, pp. 1-2, Glendale, USA, November 2010.

[35] J. W. Kolar, F. Schafmeister, S. D. Round, and H. Ertl, "Novel three-phase AC–AC sparse matrix converters," *IEEE Transactions on Power Electronics*, vol. 22, no. 5, pp. 1649–1661, 2007.

[36] S. Huang, J. Wang, C. Huang et al., "A fixed-time fractional-order sliding mode control strategy for power quality enhancement of PMSG wind turbine," *International Journal of Electrical Power & Energy Systems*, vol. 134, Article ID 107354, 2022.

[37] D. Grenier, L. A. Dessaint, O. Akhrif, Y. Bonnassieux, and B. Le Pioufle, "Experimental nonlinear torque control of a permanent-magnet synchronous motor using saliency," *IEEE Transactions on Industrial Electronics*, vol. 44, no. 5, pp. 680–687, 1997.

[38] S. Rahmani, L. Rmili, and K. Al-Haddad, "A review of indirect matrix converter topologies," *Renewable Energy and Sustainable Development*, vol. 1, no. 1, pp. 30–37, 2015.

[39] R. Matušů, "Application of fractional order calculus to control theory," *International Journal of Mathematical Models and Methods in Applied Sciences*, vol. 5, no. 7, pp. 1162–1169, 2011.

[40] C. Ma and Y. Hori, "The application of fractional order control to backlash vibration suppression," in *Proceedings of the American Control Conference*, pp. 2901–2906, Boston, MA, USA, July 2004.

[41] P. Rastogi, S. Chatterji, and D. S. Karanjkar, "Performance analysis of fractional-order controller for pH neutralization process," in *Proceedings of the 2nd International Conference on Power, Control and Embedded Systems*, pp. 1–6, Allahabad, India, December 2012.

[42] M. Khandare and J. Patil, "Review of fractional inequalities with Applications of fractional calculus," *International Journal of Advance Scientific Research and Engineering Trends*, vol. 6, no. 7, pp. 109–114, 2021.

[43] H. M. Cuong, H. Q. Dong, P. V. Trieu, and L. A. Tuan, "Adaptive fractional-order terminal sliding mode control of rubber-tired gantry cranes with uncertainties and unknown disturbances," *Mechanical Systems and Signal Processing*, vol. 154, Article ID 107601, 2021.

[44] M. E. Girgis, R. A. Fahmy, and R. I. Badr, "Optimal fractional order PID control for plasma shape, position, and current in Tokamaks," *Fusion Engineering and Design*, vol. 150, Article ID 111361, 2020.

[45] R. E. Guti´errez, J. M. Ros´ario, and J. T. MacHado, "Fractional order calculus: basic concepts and engineering applications," *Mathematical Problems in Engineering*, vol. 2010, Article ID 375858, 19 pages, 2010.

[46] I. Petr´aš, "Stability of fractional-order systems with rational orders: a survey," *Fractional Calculus and Applied Analysis*, vol. 12, no. 3, pp. 269–298, 2009.

[47] M. Karami, A. Kazemi, R. Vatankhah, and A. Khosravifard, "Adaptive fractional-order backstepping sliding mode controller design for an electrostatically actuated size-dependent microplate," *Journal of Vibration and Control*, vol. 27, no. 11-12, pp. 1353–1369, 2021.

[48] M. Al-Dhaifallah, N. Kanagaraj, and K. S. Nisar, "Fuzzy fractional order PID controller for fractional model of pneumatic pressure system," *Mathematical Problems in Engineering*, vol. 2018, Article ID 5478781, 9 pages, 2018.

[49] I. Petr´aš, "Tuning and implementation methods for fractional order controllers," *Fractional Calculus and Applied Analysis*, vol. 15, no. 2, pp. 282–303, 2012.

[50] X. Wu, Y. Xu, J. Liu, C. Lv, J. Zhou, and Q. Zhang, "Characteristics analysis and fuzzy fractional-order PID parameter optimization for primary frequency modulation of a pumped storage unit based on a multi-objective gravitational search algorithm," *Energies*, vol. 13, no. 1, pp. 137–220, 2019.

[51] T. Onyedi, A. Tepljakov, and E. Petlenkov, "FOMCONpy: fractional-order modelling and control library for Python," in *Proceedings of the IEEE 43rd International Conference on Telecommunications and Signal Processing*, pp. 239–245, Milan, Italy, July 2020.

[52] I. Petras, A. Tepljakov, E. Petlenkov, and J. Belikov, "FOMCON toolbox for modeling, design and implementation of fractional-order control systems," in *Applications in Control*, pp. 211–236, Walter de Gruyter Press, Berlin, Germany, 1th edition, 2019.

[53] L. Liu, D. Xue, and S. Zhang, "General type industrial temperature system control based on fuzzy fractional-order PID controller," *Complex & Intelligent Systems*, vol. 2021, pp. 1–13, 2021.

[54] G. Sahoo, R. K. Sahu, N. R. Samal, and S. Panda, "Analysis of type-2 fuzzy fractional-order PD-PI controller for frequency stabilisation of the micro-grid system with real-time simulation," *International Journal of Sustainable Energy*, vol. 41, no. 5, pp. 412–433, 2021.

[55] P. Swethamarai, P. Lakshmi, and S. G. Prassad, "Whale-optimized fuzzy-fractional order controller-based automobile suspension model," *Engineering Optimization*, vol. 2021, pp. 1–21, 2021.